Wefer, G., Berger, W.H., and Richter, C. (Eds.)
Proceedings of the Ocean Drilling Program, Scientific Results Volume 175

8. Data Report: Magnetic Properties of Core Sediments from Site 1081 (Walvis Ridge), Leg 175[1]

Gina Marie Frost[2] and Toshitsugu Yamazaki[3]

ABSTRACT

Magnetic properties are reported for samples from sediment cores recovered at Site 1081 on the Walvis Ridge (~20°S) during Leg 175 of the Ocean Drilling Program. Rock magnetic data indicate that the remanence is carried by low-coercivity minerals. Paramagnetic and diamagnetic minerals dominate the susceptibility. Comparison of measurements made aboard ship with those made on shore after the cruise indicate a marked loss of magnetization, probably due to dissolution of some magnetic minerals after core recovery similar to that which has occurred at other Leg 175 sites.

INTRODUCTION

Site 1081 (Fig. **F1**) (19°37.2′S, 11°19.2′E) is the shallow-water (793.8 m) site of the Walvis Ridge/Walvis Basin Group, which includes Ocean Drilling Program (ODP) Sites 1082 and 1083 and Deep Sea Drilling Project (DSDP) Sites 362 and 532 (Shipboard Scientific Party, 1998).

In general, the sediments at Site 1081 consist of clay with varying amounts of diatoms, nannofossils, foraminifers, and radiolarians; below 390 meters below seafloor (mbsf) the sediments are primarily a clayey nannofossil ooze (Shipboard Scientific Party, 1998). Concentrations of calcium carbonate and organic carbon are high to ~77 mbsf (average = 31 and 5 wt%, respectively); between 77 and 230 mbsf, concentrations of carbonate decrease to an average of 8 wt%, but organic carbon concentration remains high (maximum = 8.2 wt%; average = 5.21 wt%)

F1. Site map showing the location of Site 1081, p. 7.

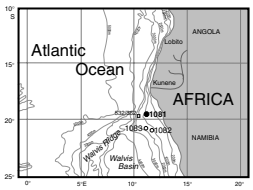

[1]Frost, G.M., and Yamazaki, T., 2001. Data report: Magnetic properties of core sediments from Site 1081 (Walvis Ridge), Leg 175. *In* Wefer, G., Berger, W.H., and Richter, C. (Eds.), *Proc. ODP, Sci. Results,* 175, 1–17 [Online]. Available from World Wide Web: <http://www-odp.tamu.edu/publications/175_SR/VOLUME/CHAPTERS/SR175_08.PDF>. [Cited YYYY-MM-DD]
[2]Hawaii Institute of Geophysics and Planetology, School of Ocean and Earth Science and Technology, University of Hawaii, Honolulu HI 96822, USA. Present address: Central Oregon Community College, Bend OR 97702, USA. **gfrost@cocc.edu**
[3]Geological Survey of Japan, 1-1-3 Higashi, Tsukuba, Ibaraki 305-8567, Japan.

Initial receipt: 21 February 2000
Acceptance: 14 September 2000
Web publication: 16 April 2001
Ms 175SR-206

(Shipboard Scientific Party, 1998). Between 230 and 390 mbsf, carbonate concentrations increase to an average of 18 wt% with 3.34 wt% organic carbon (Shipboard Scientific Party, 1998). Below 390 mbsf, carbonate concentrations average 30 wt% with 2.18 wt% organic carbon. Intervals of dolomitized clay are present between 137 and 183 mbsf (Shipboard Scientific Party, 1998). Sedimentation rates for the reported sample set are high, averaging between 70 and 150 m/m.y. (Shipboard Scientific Party, 1998). The oldest sediments are late Miocene in age based on paleontologic data (Shipboard Scientific Party, 1998). A complete magnetostratigraphy for the uppermost 120 mbsf was determined aboard ship (Shipboard Scientific Party, 1998).

Environmental processes affect the magnetic properties of sediments (Hall et al., 1997; Karlin, 1990a, 1990b; Karlin and Levi, 1983, 1985; Karlin et al., 1987; Roberts and Turner, 1993; Torii, 1997), particularly in areas of high productivity with a high organic carbon influx (Bloemendal et al., 1992; Hartl et al., 1995; Mead et al., 1986; Tarduno, 1994, 1995). Of particular concern are diagenetic changes that occur after core recovery (Richter et al., 1999; Roberts et al., 1999; Yamazaki et al., 2000), which affects the integrity of paleomagnetic and rock magnetic records of marine sediments.

In this paper, the following magnetic properties are reported for sediments recovered from Site 1081: remanent intensity variation, magnetic susceptibility, anhysteretic and isothermal remanence acquisition and demagnetization, and hysteresis behavior.

MATERIALS AND METHODS

Remanent magnetization after alternating field (AF) demagnetization up to 20 mT of all archive-half core sections from Site 1081 was measured at 5-cm intervals aboard ship using a 2G Enterprises pass-through cryogenic magnetometer (Wefer, Berger, and Richter, et al., 1998); selected working-half core sections were also measured aboard ship (Sections 175-1081C-9H-5, 10H-3, and 11H-3) (Shipboard Scientific Party, 1998).

A total of 245 discrete samples, taken aboard ship from working-half core sections at one 7-cm^3 cube per section for Hole 1081A, were measured at the Geological Survey of Japan. An additional 101 discrete samples (10-cm^3 cubes) and U-channels, taken postcruise, were measured at the Hawaii Institute of Geophysics and Planetology (HIGP).

Equipment used at the HIGP paleomagnetics laboratory included a an in-line degaussing system capable of peak alternating current (AC) fields up to 120 mT (accuracy = ±1%), an in-line anhysteretic remanence magnetizer, and a 2G Enterprises Model 760R cryogenic magnetometer housed in a shielded room and equipped with an automated sample handler system, which accommodates as many as eight discrete samples per tray or U-channels as long as 150 cm. Other equipment used included an ASC Model IM-10 impulse magnetizer for imparting isothermal remanent magnetization (IRM) to discrete samples and a Kappabridge KLY-2 and Minikappa KLF-3 for discrete sample susceptibility measurements, including temperature variation.

For discrete samples, intensity of natural remanent magnetization (NRM) and volume susceptibility were measured prior to AF demagnetization. After AF demagnetization, the acquisition behavior of anhysteretic remanent magnetization (ARM) was studied for 101 samples. The AF was progressively increased from 0 to 100 mT in a direct current

(DC) bias field of 0.10 mT. Acquired remanence was measured between steps. The ARM was then AF demagnetized so the demagnetization behavior could be compared with that of NRM and IRM.

The acquisition behavior of IRM was studied for 15 samples. The DC field was progressively increased from 0 to 1.2 T; the IRM was measured between steps. Saturation IRM (SIRM) was estimated from the remanent magnetization at 1.2 T. A reversed-field IRM at 300 mT was imparted after growth and measurement of IRM, after which SIRM was again imparted and AF demagnetized. Hysteresis data were measured at room temperature using a MicroMag Model 2900 alternating gradient magnetometer.

RESULTS

Data for discrete samples from Hole 1081C are summarized in Table T1. NRM intensities range from 2.68 × 10^{-5} to 7.67 × 10^{-4} A/m (mean = 1.51 × 10^{-4} A/m), whereas remanent intensities after AF demagnetization at 20 mT vary from 4.66 × 10^{-6} to 1.95 × 10^{-4} A/m (mean = 4.13 × 10^{-5} A/m). ARM intensities acquired during AF demagnetization at 100 mT range from 1.18 × 10^{-3} to 8.45 × 10^{-3} A/m (mean = 2.91 × 10^{-3} A/m). SIRM intensities range from 2.46 × 10^{-2} to 6.71 × 10^{-2} A/m (mean = 4.51 × 10^{-2} A/m). Backfield IRMs induced at –0.3 T range from 2.26 × 10^{-2} to 6.03 × 10^{-2} A/m (mean = 4.10 × 10^{-2} A/m). Susceptibility values for discrete samples measured postcruise range from 1 × 10^{-6} to 39 × 10^{-6} SI (mean = 19 × 10^{-6} SI). Complete data from all measured discrete samples and U-channels are available from the ODP Data Librarian; long-core data measured aboard ship are available from the ODP online database.

Figure F2 illustrates ARM acquisition curves and the demagnetization behavior of NRM, ARM, and SIRM for selected discrete samples from Hole 1081C. The median destructive field (MDF) for NRM data varies between ~5 and 40 mT. During ARM acquisition, normalized intensity values (J/Jo) gradually increase over a broad range of peak AF fields; saturation of ARM is not achieved until ~80 mT for all measured samples. Demagnetization of ARM shows MDF values between 10 and 20 mT downhole to Sample 175-1081C-8H-3, 86–88 cm, with the first and shallowest sample (175-1081C-1H-3, 98–100 cm) showing an MDF value near 25 mT. The remaining (and progressively deeper) samples show generally higher MDF values between 25 and 30 mT. The last sample shows an MDF value of 20 mT. MDF values for demagnetization of SIRM are consistently between ~30 and 40 mT.

IRM acquisition curves are shown in Figure F3. The similarity in the shapes of all 15 curves is striking; all show sharply increasing intensity values below 0.1 T with near saturation of IRM achieved by 0.3 T. S ratios (Bloemendal et al., 1992) are uniformly very high (Fig. F4) (mean = 0.96; maximum = 0.96; minimum = 0.92; standard deviation = 0.01), which indicates a higher proportion of low-coercivity magnetic minerals relative to high-coercivity minerals.

Figure F5 illustrates the temperature dependence of susceptibility for selected discrete samples. Throughout the heating and cooling phases of the experiment, susceptibility values remain extremely low (10^{-5}–10^{-6} SI). Susceptibility values were negative throughout the heating phase of the experiment for all measured samples, which is characteristic for diamagnetic minerals. For two samples (175-1081C-3H-2, 100–102 cm, and 175-1081C-10H-3, 74–76 cm), the susceptibility increased signifi-

T1. Summary of rock magnetic data, p. 16.

F2. Normalized intensities during ARM acquisition and ARM, NRM, and SIRM demagnetization, p. 8.

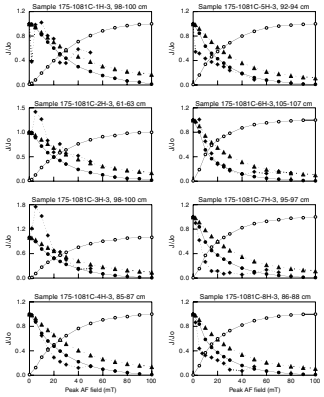

F3. Intensity vs. applied DC field during progressive IRM acquisition, p. 10.

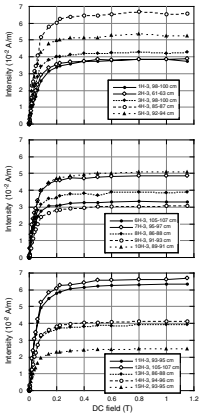

F4. S ratios, p. 11.

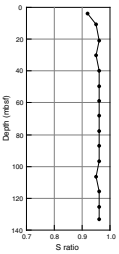

cantly during heating between ~225°–300°C and 250°–300°C, respectively, indicating the formation of a new magnetic mineral. Above these temperatures, susceptibility values drop and thereafter remain low up to the maximum temperature. A gradual increase occurs up to ~475°C during heating for Sample 175-1081C-15H-3, 52–54 cm, but no dramatic increase like that observed in the previous samples is apparent.

During cooling of all three samples, susceptibility values increased sharply beginning at ~575°, 525°, and 580°C, respectively, and continued to increase to positive values before peaking near 425°, 225°, and 350°C, respectively (Fig. F5). Positive susceptibility values persist for the remainder of the cooling cycle, decreasing gradually below ~200°C for Sample 175-1081C-3H-2, 100–102 cm, and shortly after peaking for the remaining two samples.

Hysteresis data are dominated by paramagnetic behavior (Fig. F6) with no evidence for a ferrimagnetic component after correction for paramagnetic behavior.

NRM intensity data from Holes 1081A and 1081C show inconsistencies between data collected on the ship and data collected on shore after the cruise (Fig. F7A). Discrete samples from Hole 1081A show intensity values that are generally on the same order of magnitude as shipboard data, with notable exceptions. Between ~120 and 170 mbsf, intensity values measured up to two orders of magnitude higher than shipboard data collected from long cores. The intensity values of discrete samples above ~50 mbsf are lower than, but on the same order of magnitude as, shipboard data. Intensity values of discrete samples below ~320 mbsf are higher than, but on the same order of magnitude as, shipboard data.

Discrete samples from Hole 1081C show intensity values up to two orders of magnitude lower than shipboard data collected from long cores (Fig. F7A). The marked intensity loss is probably due to a greater time lag between measurement of long cores and discrete samples at this hole than at Hole 1081A.

U-channel intensity data from two sections are consistent with shipboard data from long cores above ~54.9 mbsf but diverge from shipboard data below this depth (Fig. F7B).

Susceptibility data for discrete samples at Hole 1081C are up to one order of magnitude lower than shipboard whole-core susceptibility measurements (Fig. F8).

CONCLUSION

Rock magnetic data indicate that the remanence is carried by low coercivity minerals, but the susceptibility is dominated by diamagnetic and paramagnetic minerals. The observed general loss of magnetization is probably due to dissolution of some magnetic minerals after core recovery at Site 1081, which is consistent with data from other Leg 175 sites (Yamazaki et al., 2000).

ACKNOWLEDGMENTS

We thank all participants of ODP Leg 175, Captain Anthony Ribbens and the crew of the *JOIDES Resolution,* and ODP personnel at the Bremen Core Repository for their cooperation in making this work possi-

F5. Temperature dependence of susceptibility (K), p. 12.

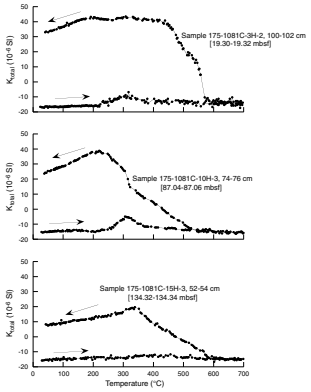

F6. Hysteresis loops, p. 13

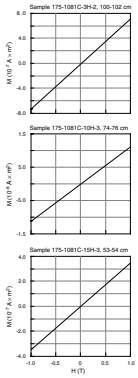

F7. Intensity vs. depth, p. 14

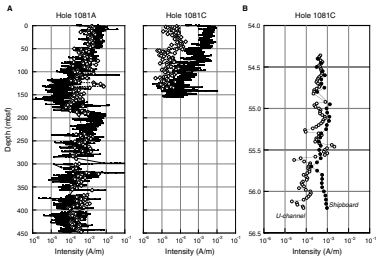

F8. Volume susceptibility vs. depth, p. 15.

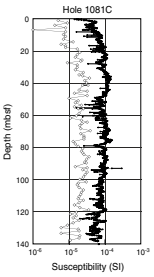

ble. We thank Dr. N. Ishikawa at Kyoto University for hysteresis measurements. All samples were provided by ODP. This work was supported in part by grants from the Joint Oceanographic Institutions/U.S. Science Support Program (JOI/USSSP; 175-F000738 and 175-F000826).

REFERENCES

Bloemendal, J., King, J.W., Hall, F.R., and Doh, S.-J., 1992. Rock magnetism of late Neogene and Pleistocene deep-sea sediments: relationship to sediment source, diagenetic processes, and sediment lithology. *J. Geophys. Res.,* 97:4361–4375.

Hall, F.R., Cisowski, S., and John, S., 1997. Data report: Environmental rock-magnetic evidence of authigenic-magnetic mineral formation/preservation (Amazon Fan). *In* Flood, R.D., Piper, D.J.W., Klaus, A., and Peterson, L.C. (Eds.), *Proc. ODP, Sci. Results,* 155: College Station, TX (Ocean Drilling Program), 251–270.

Hartl, P., Tauxe, L., and Herbert, T., 1995. Earliest Oligocene increase in South Atlantic productivity as interpreted from "rock magnetics" at Deep Sea Drilling Site 522. *Paleoceanography,* 10:311–326.

Karlin, R., 1990a. Magnetic diagenesis in marine sediments from the Oregon continental margin. *J. Geophys. Res.,* 95:4405–4419.

————, 1990b. Magnetite mineral diagenesis in suboxic sediments at Bettis Site W-N, NE Pacific Ocean. *J. Geophys. Res.,* 95:4421–4436.

Karlin, R., and Levi, S., 1983. Diagenesis of magnetic minerals in recent hemipelagic sediments. *Nature,* 303:327–330.

————, 1985. Geochemical and sedimentological control of the magnetic properties of hemipelagic sediments. *J. Geophys. Res.,* 90:10373–10392.

Karlin, R., Lyle, M., and Heath, G.R., 1987. Authigenic magnetite formation in suboxic marine sediments. *Nature,* 326:490–493.

Mead, G.A., Tauxe, L., and LaBrecque, J.L., 1986. Oligocene paleoceanography of the South Atlantic: paleoclimatic implications of sediment accumulation rates and magnetic susceptibility. *Paleoceanography,* 1:273–284.

Richter, C., Hayashida, A., Guyodo, Y., Valet, J.-P., and Verosub, K.L., 1999. Magnetic intensity loss and core diagenesis in long-core samples from the East Cortez Basin and the San Nicolas Basin (California Borderland). *Earth, Planets Space,* 51:329–336.

Roberts, A.P., Stoner, J.S., and Richter, C., 1999. Diagenetic magnetic enhancement of sapropels from the eastern Mediterranean Sea. *Mar. Geol.,* 153:103-116.

Roberts, A.P., and Turner, G.M., 1993. Diagenetic formation of ferrimagnetic iron sulphide minerals in rapidly deposited marine sediments, South Island, New Zealand. *Earth Planet. Sci. Lett.,* 115:257–273.

Shipboard Scientific Party, 1998. Site 1081. *In* Wefer, G., Berger, W.H., and Richter, C., et al., *Proc. ODP, Init. Repts.,* 175: College Station, TX (Ocean Drilling Program), 223–272.

Tarduno, J.A., 1994. Temporal trends of magnetic dissolution in the pelagic realm: gauging paleoproductivity? *Earth Planet. Sci. Lett.,* 123:39–48.

————, 1995. Superparamagnetism and reduction diagenesis in pelagic sediments: enhancement or depletion? *Geophys. Res. Lett.,* 22:1337–1340.

Torii, M., 1997. Low-temperature oxidation and subsequent downcore dissolution of magnetite in deep-sea sediments, ODP Leg 161 (Western Mediterranean). *J. Geomagn. Geoelect.,* 49:1233–1245.

Wefer, G., Berger, W.H., and Richter, C., et al., 1998. *Proc. ODP, Init. Repts.,* 175: College Station, TX (Ocean Drilling Program).

Yamazaki, T., Solheid, P.A., and Frost, G.M., 2000. Rock magnetism of sediments in the Angola-Namibia upwelling system with special reference to loss of magnetization after core recovery. *Earth, Planets Space,* 52:329–336.

Figure F1. Site map showing the location of Site 1081 along the western coast of Africa in the southeast Atlantic Ocean. Also shown are the other Walvis Ridge/Walvis Basin group sites: Sites 1082 and 1083 (Leg 175) and DSDP Sites 362 and 532 (Legs 40 and 75, respectively).

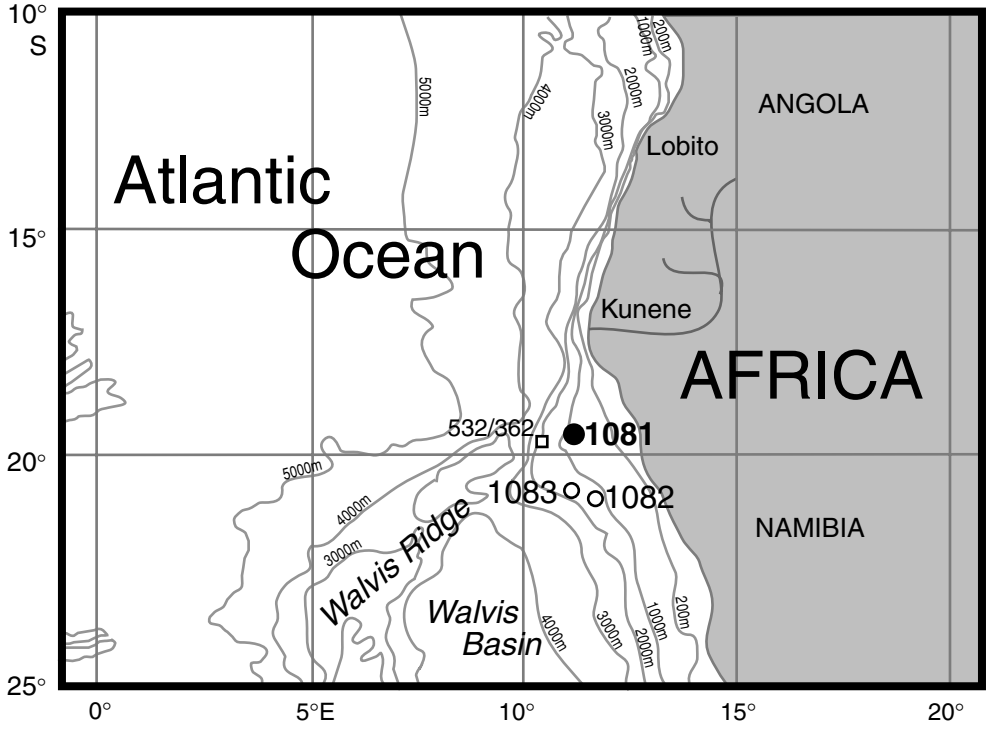

Figure F2. Normalized intensities (J/Jo) during progressive ARM acquisition (open circles), ARM demagnetization (solid circles), NRM demagnetization (diamonds), and SIRM demagnetization (triangles). Samples 175-1081C-10H-3, 89–91 cm, and 175-1081C-11H-3, 93–95 cm, were previously demagnetized to 20 mT as part of shipboard measurement of long cores prior to shorebased measurements. (Continued on next page.)

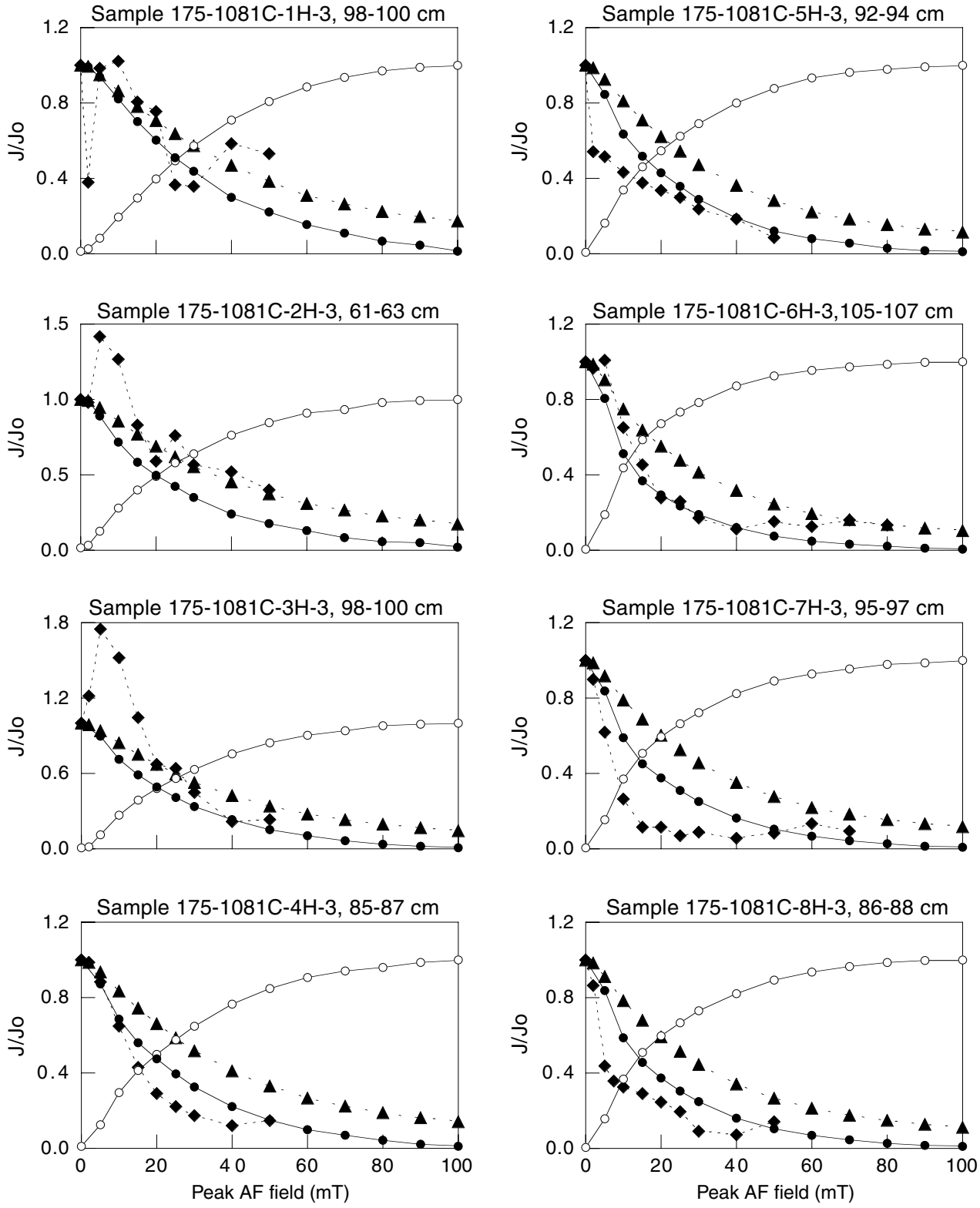

Figure F2 (continued).

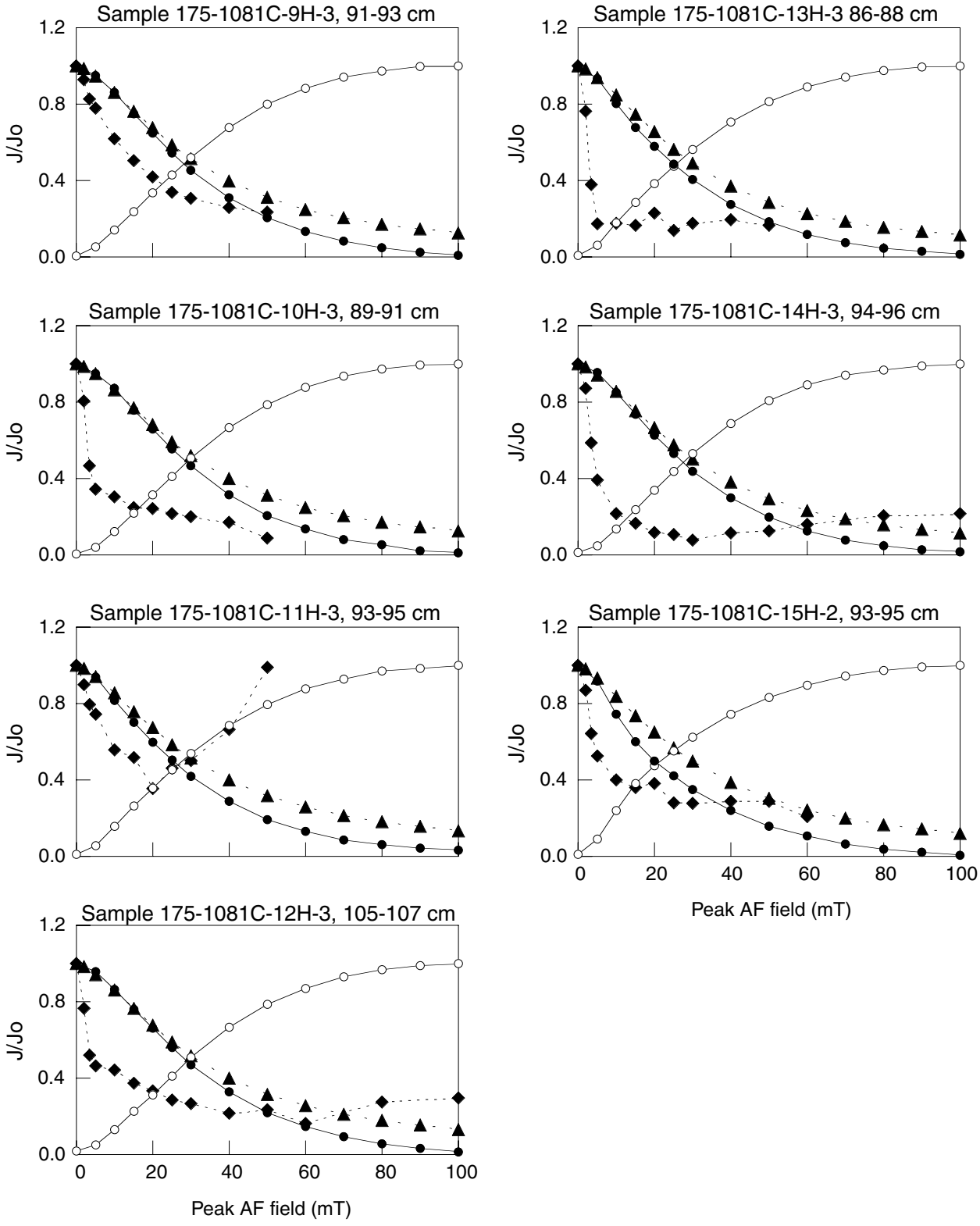

Figure F3. Intensity vs. applied DC field during progressive IRM acquisition for discrete samples from Hole 1081C.

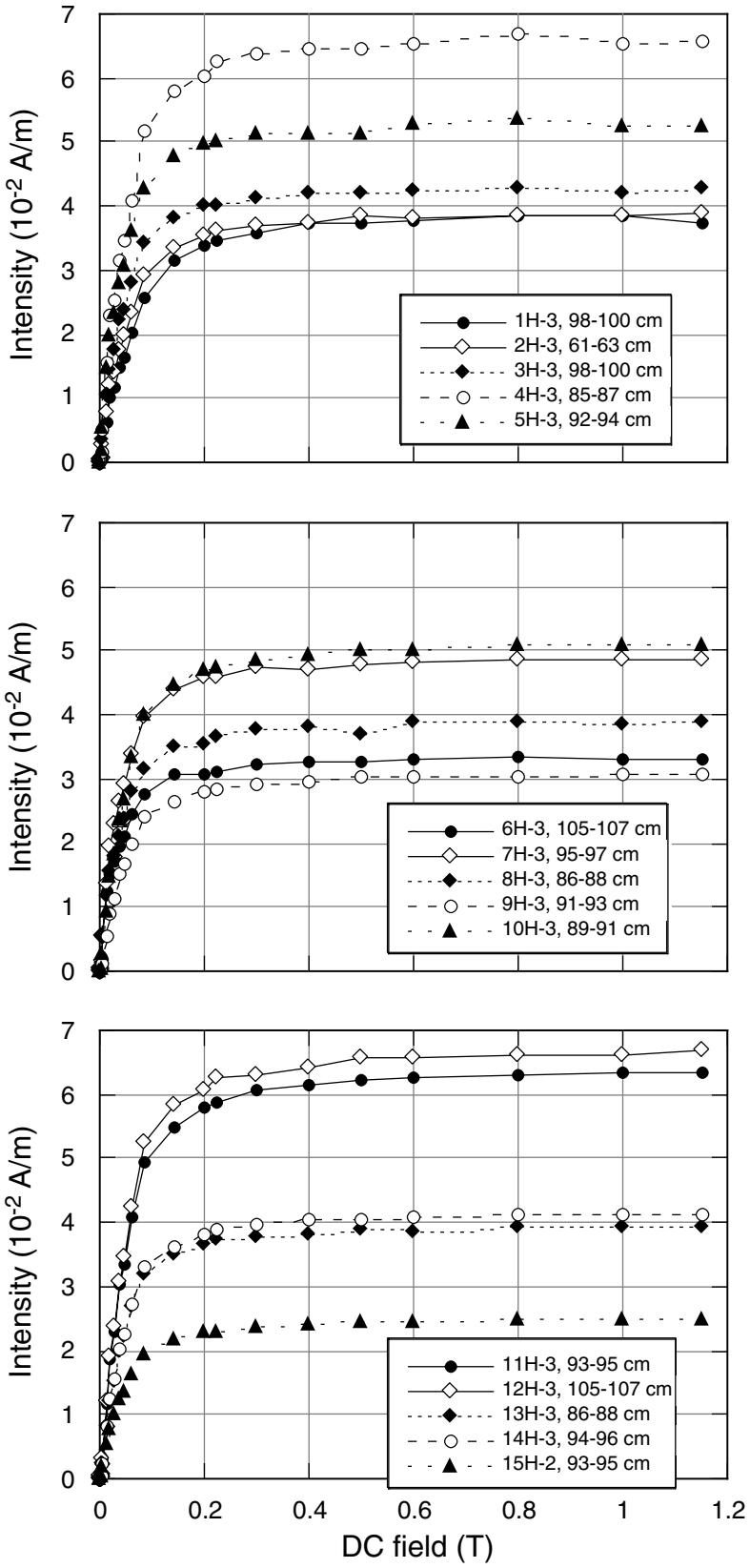

Figure F4. S ratios for discrete samples at Hole 1081C.

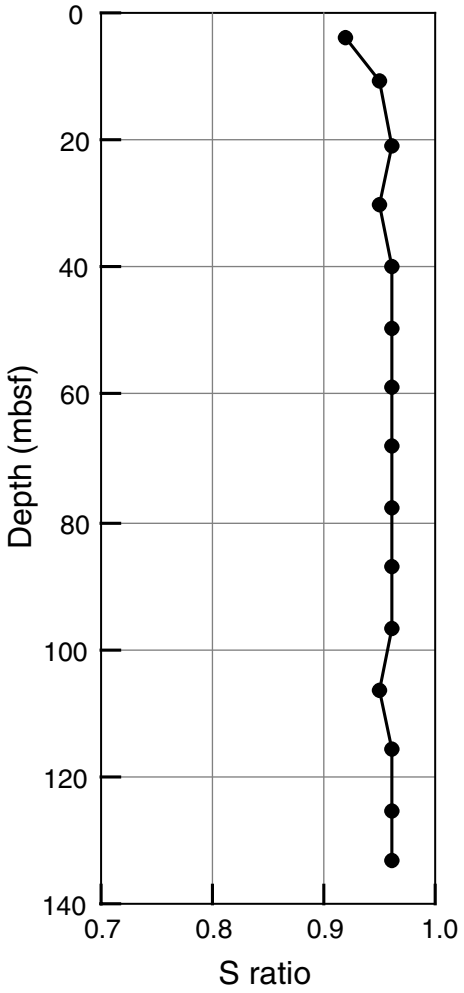

Figure F5. Temperature dependence of susceptibility (K) for discrete samples from Hole 1081C. The heating curve is indicated by the right-pointing arrow; the cooling curve, by the left-pointing arrow. Volume susceptibilities data are corrected for average furnace value.

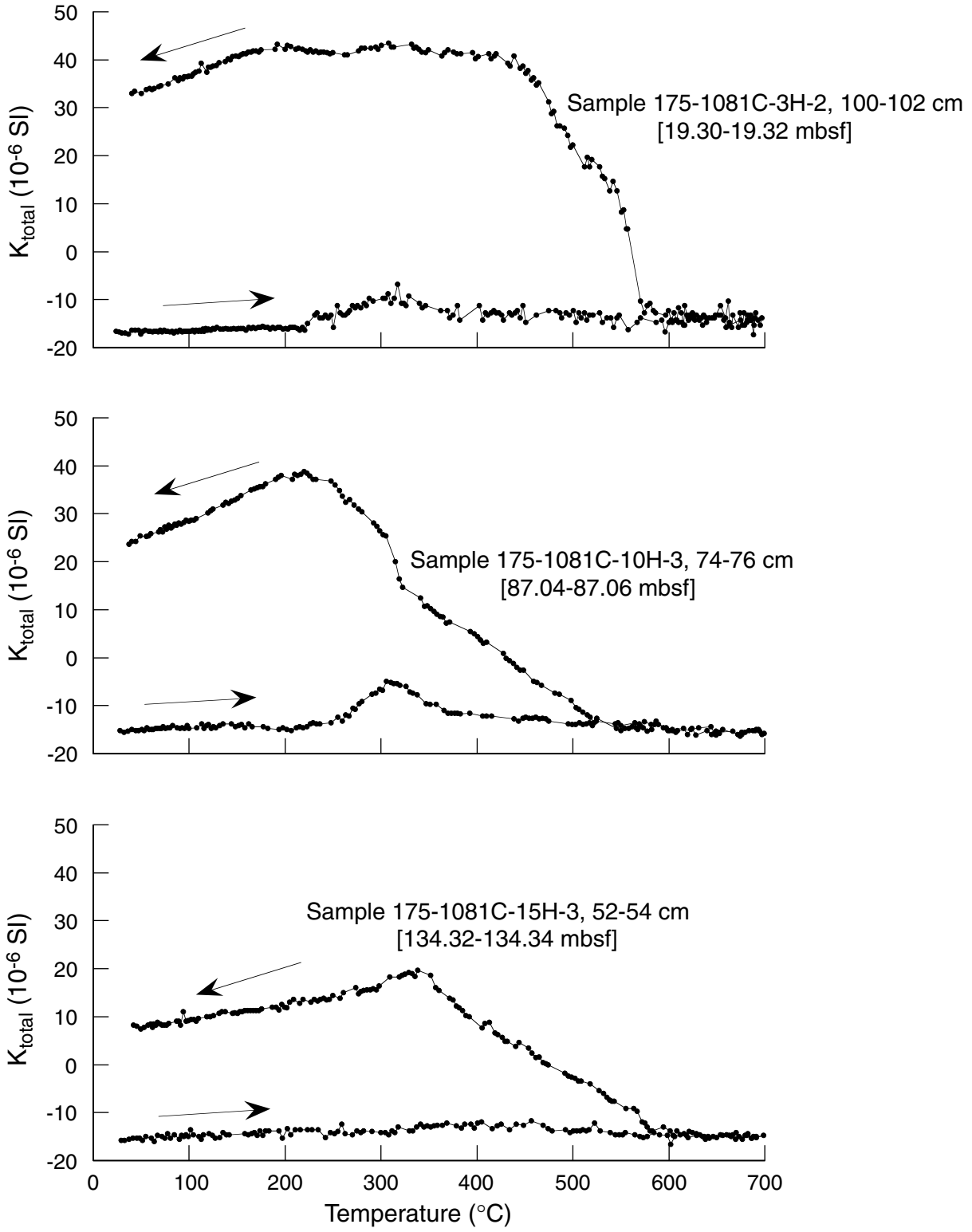

Figure F6. Hysteresis loops for discrete samples from Hole 1081C. M = magnetic moment, H = applied field.

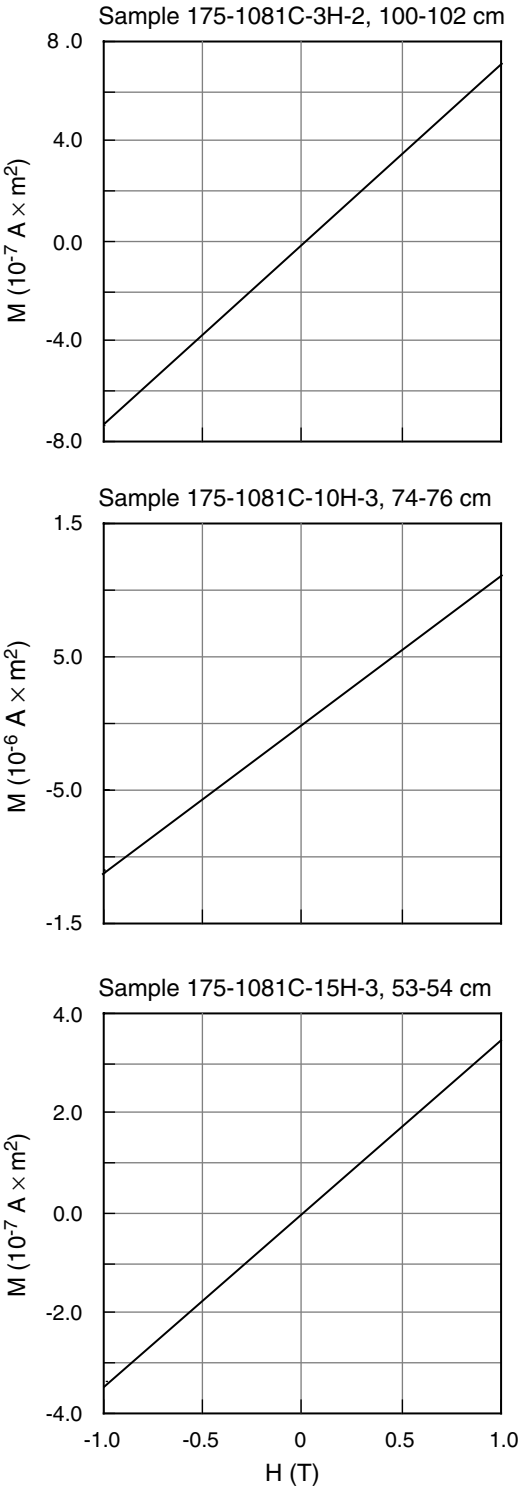

Figure F7. Intensity vs. depth at Holes 1081A and 1081C. All data shown are after AF demagnetization at 20 mT. **A.** Shipboard long-core data are shown as connected solid squares; discrete sample data measured on shore are shown as open diamonds. **B.** Shipboard long-core data are shown as connected solid circles; U-channel data measured on shore are shown as open circles.

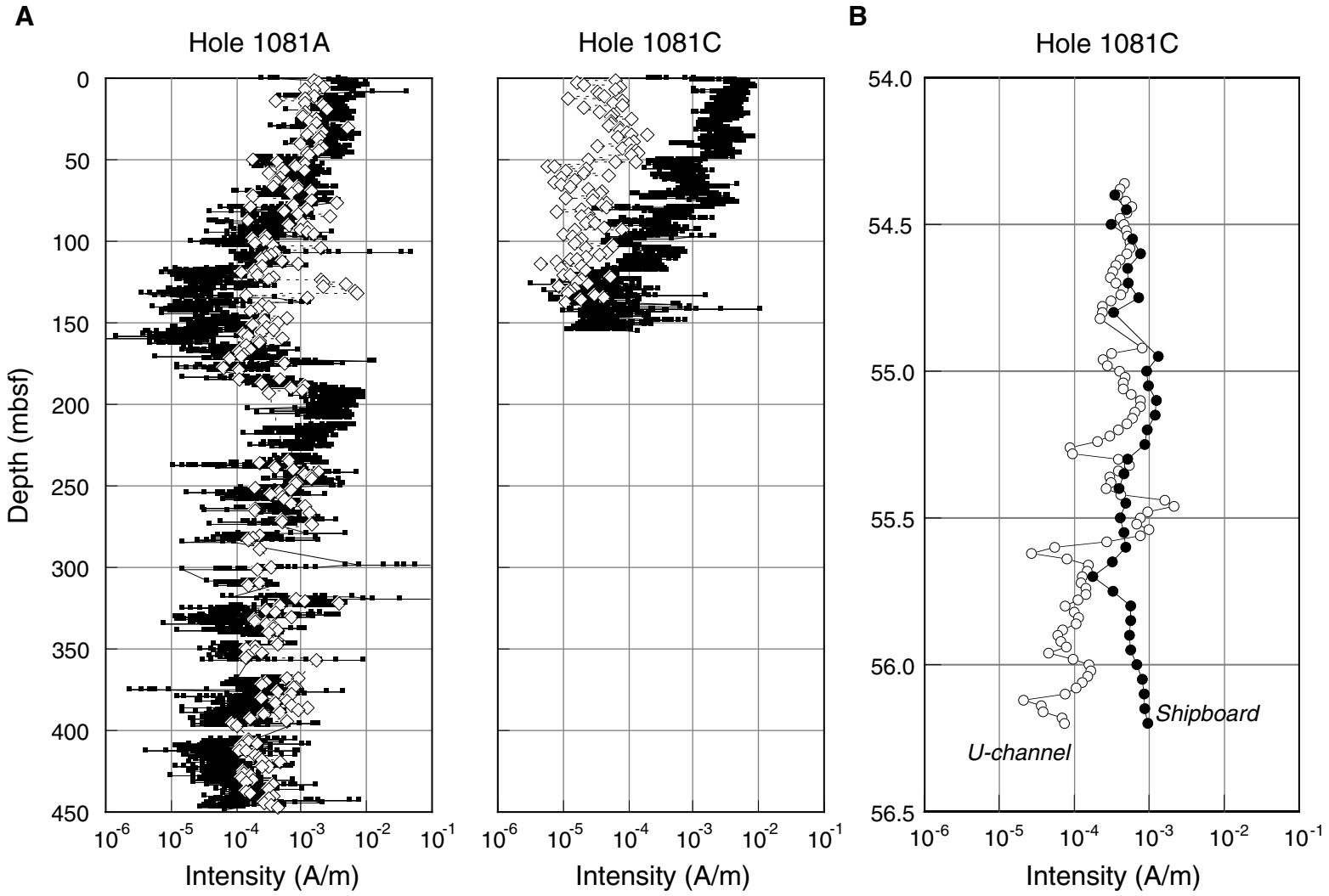

Figure F8. Volume susceptibility vs. depth at Hole 1081C. Shipboard whole-core data are shown as connected solid squares; discrete sample data are shown as open diamonds.

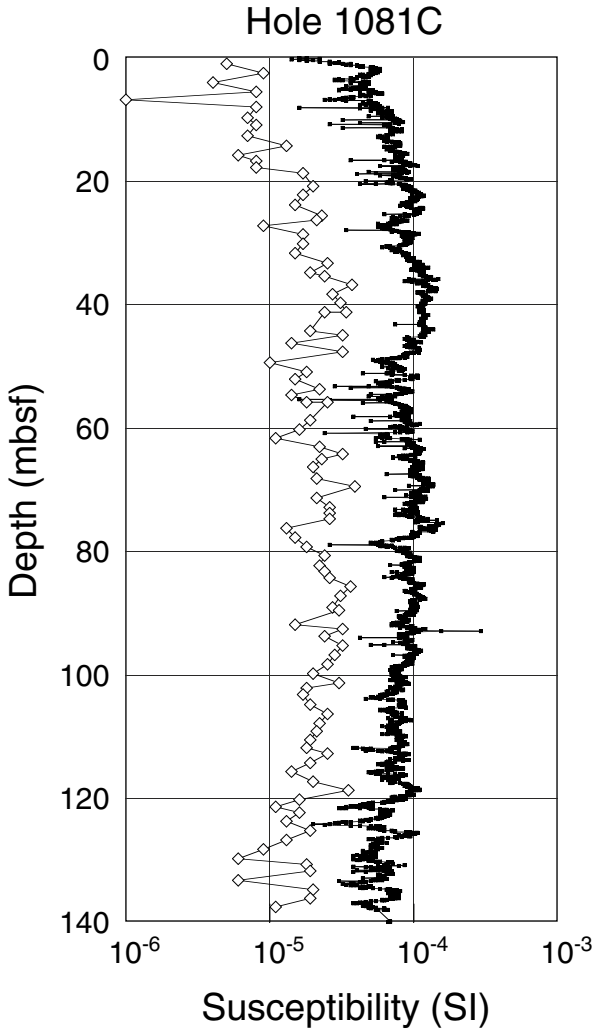

Table T1. Summary of rock magnetic data, Hole 1081C. (See table note. Continued on next page.)

Core, section, interval (cm)	Depth (mbsf)	J (G)	NRM (A/m)	RM20 (A/m)	ARM100 (A/m)	SIRM (A/m)	IRM–0.3 (A/m)	K (10^{-6}SI)
175-1081C-								
1H-1, 100-103	1.02	1.23E-07	1.23E-04	6.47E-05	1.77E-03			5
1H-2, 100-102	2.51	6.86E-08	6.86E-05	1.64E-05	1.87E-03			9
1H-3, 98-100	3.99	2.79E-08	2.79E-05	2.11E-05	1.35E-03	3.83E-02	3.24E-02	4
1H-4, 98-100	5.49	8.60E-08	8.60E-05	7.53E-05	1.22E-03			8
1H-5, 80-82	6.81	1.56E-07	1.56E-04	6.51E-05	1.46E-03			1
2H-1, 70-72	8.01	2.08E-07	2.08E-04	3.43E-05	1.91E-03			8
2H-2, 98-100	9.79	8.60E-08	8.60E-05	3.55E-05	1.78E-03			7
2H-3, 61-63	10.92	7.20E-08	7.20E-05	4.23E-05	2.18E-03	3.94E-02	3.57E-02	8
2H-4, 81-83	12.62	6.41E-08	6.41E-05	1.20E-05	1.56E-03			7
2H-5, 98-100	14.29	2.45E-07	2.45E-04	8.27E-05	2.89E-03			13
2H-6, 98-100	15.79	1.56E-07	1.56E-04	5.95E-05	2.03E-03			6
2H-7, 43-45	16.74	1.87E-07	1.87E-04	8.10E-05	2.47E-03			8
3H-1, 98-100	17.79	1.08E-07	1.08E-04	2.14E-05	2.10E-03			8
3H-2, 40-42	18.71	7.28E-08	7.28E-05	2.11E-05	1.33E-03			17
3H-3, 98-100	20.79	5.49E-08	5.49E-05	3.68E-05	2.64E-03	4.32E-02	3.96E-02	20
3H-4, 86-88	22.17	1.16E-07	1.16E-04	5.75E-05	2.75E-03			17
3H-5, 98-100	23.79	2.60E-07	2.60E-04	5.65E-05	2.99E-03			15
3H-6, 91-93	25.55	6.50E-07	6.50E-04	1.14E-04	5.87E-03			23
3H-7, 43-45	26.24	1.82E-07	1.82E-04	5.47E-05	2.91E-03			21
4H-1, 98-100	27.29	1.01E-07	1.01E-04	5.34E-05	2.47E-03			9
4H-2, 82-84	28.63	6.85E-08	6.85E-05	4.90E-05	4.19E-03			17
4H-3, 85-87	30.16	2.55E-07	2.55E-04	7.41E-05	4.02E-03	6.71E-02	6.03E-02	17
4H-4, 84-86	31.65	2.75E-07	2.75E-04	7.24E-05	3.56E-03			15
4H-5, 100-102	33.31	1.27E-07	1.27E-04	9.40E-05	3.62E-03			25
4H-6, 102-104	34.83	2.75E-07	2.75E-04	1.09E-04	5.15E-03			19
4H-7, 14-16	35.34	7.67E-07	7.67E-04	1.95E-04	8.45E-03			24
5H-1, 93-95	36.74	1.70E-07	1.70E-04	6.94E-05	3.11E-03			37
5H-2, 98-100	38.29	5.27E-07	5.27E-04	1.18E-04	4.92E-03			27
5H-3, 92-94	39.73	3.11E-07	3.11E-04	1.05E-04	4.04E-03	5.32E-02	4.88E-02	31
5H-4, 96-98	41.27	1.82E-07	1.82E-04	3.27E-05	2.95E-03			34
5H-5, 84-86	41.27	3.39E-07	3.39E-04	7.91E-05	3.48E-03			24
5H-6, 98-100	44.29	5.31E-07	5.31E-04	1.09E-04	4.51E-03			19
5H-7, 18-20	44.99	3.74E-07	3.74E-04	1.35E-04	4.06E-03			32
6H-1, 90-92	46.21	4.19E-07	4.19E-04	1.40E-04	4.80E-03			14
6H-2, 87-89	47.68	2.43E-07	2.43E-04	1.13E-04	3.60E-03			32
6H-3, 105-107	49.36	8.68E-08	8.68E-05	2.41E-05	3.58E-03	3.32E-02	3.08E-02	10
6H-4, 111-113	50.92	1.91E-07	1.91E-04	1.30E-04	1.74E-03			18
6H-5, 77-79	52.08	1.70E-07	1.70E-04	6.55E-05	4.78E-03			15
6H-6, 96-98	53.77	1.34E-07	1.34E-04	5.60E-06	3.74E-03			22
6H-7, 30-32	54.61	1.83E-07	1.83E-04	7.61E-06	6.91E-03			14
7H-1, 100-102	55.81	3.87E-08	3.87E-05	2.19E-05	3.23E-03			18
7H-2, 90-92	55.81	1.15E-07	1.15E-04	1.10E-05	3.14E-03			25
7H-3, 95-97	58.76	1.87E-07	1.87E-04	2.12E-05	4.02E-03	4.99E-02	4.55E-02	19
7H-4, 86-88	60.17	7.52E-08	7.52E-05	4.92E-05	2.08E-03			16
7H-5, 82-84	61.63	6.45E-08	6.45E-05	9.72E-06	1.59E-03			11
7H-6, 67-69	62.98	9.59E-08	9.59E-05	1.46E-05	2.49E-03			22
7H-7, 33-35	64.14	5.41E-08	5.41E-05	7.34E-06	3.73E-03			32
8H-1, 72-74	65.03	8.60E-08	8.60E-05	9.53E-06	2.27E-03			23
8H-2, 56-58	66.37	5.96E-08	5.96E-05	1.30E-05	2.61E-03			20
8H-3, 86-88	68.17	1.01E-07	1.01E-04	2.46E-05	3.41E-03	3.89E-02	3.55E-02	21
8H-4, 70-72	69.51	1.17E-07	1.17E-04	3.81E-05	3.39E-03			39
8H-5, 102-104	71.33	6.97E-08	6.97E-05	3.64E-05	2.28E-03			21
8H-6, 96-98	72.77	8.39E-08	8.39E-05	2.94E-05	3.01E-03			26
8H-7, 50-52	73.81	5.27E-08	5.27E-05	1.10E-05	3.67E-03			26
9H-1, 89-91	74.70	8.19E-08	8.19E-05	2.92E-05	3.00E-03			26
9H-2, 97-99	76.28	1.64E-07	1.64E-04	4.58E-05	3.67E-03			13
9H-3, 91-93	77.72	9.28E-08	9.28E-05	3.87E-05	1.62E-03	3.02E-02	2.78E-02	15
9H-4, 96-98	79.27	1.41E-07	1.41E-04	4.73E-05	2.73E-03			18
9H-5, 88-90	80.69	3.66E-08	3.66E-05	2.01E-05	2.11E-03			24
9H-6, 93-95	82.24	1.31E-07	1.31E-04	7.78E-06	3.52E-03			22
9H-7, 37-39	83.18	1.83E-07	1.83E-04	2.54E-05	3.77E-03			24
10H-1, 94-96	84.25	1.60E-07	1.60E-04	2.01E-05	3.27E-03			26
10H-2, 89-91	85.70	1.90E-07	1.90E-04	2.58E-05	4.81E-03			36
10H-3, 89-91	87.20	1.07E-07	1.07E-04	2.56E-05	2.59E-03	5.04E-02	4.59E-02	31
10H-4, 119-121	89.00	8.95E-08	8.95E-05	2.24E-05	2.21E-03			27
10H-5, 21-23	89.52	1.02E-07	1.02E-04	3.05E-05	4.11E-03			30
10H-6, 100-102	91.81	1.44E-07	1.44E-04	4.22E-05	3.71E-03			15

Table T1 (continued).

Core, section, interval (cm)	Depth (mbsf)	J (G)	NRM (A/m)	RM20 (A/m)	ARM100 (A/m)	SIRM (A/m)	IRM–0.3 (A/m)	K (10^{-6}SI)
10H-7, 23-25	92.54	1.98E-07	1.98E-04	8.04E-05	7.04E-03			32
11H-1, 93-95	93.74	1.56E-07	1.56E-04	1.49E-05	3.76E-03			24
11H-2, 94-96	95.25	2.15E-07	2.15E-04	1.01E-05	4.80E-03			32
11H-3, 93-95	96.74	3.98E-08	3.98E-05	1.40E-05	3.15E-03	6.28E-02	5.75E-02	28
11H-4, 91-93	98.22	1.07E-07	1.07E-04	1.90E-05	2.56E-03			25
11H-5, 92-94	99.73	1.15E-07	1.15E-04	1.65E-05	1.98E-03			20
11H-6, 97-99	101.28	1.43E-07	1.43E-04	1.50E-05	2.92E-03			30
11H-7, 31-33	102.12	4.56E-08	4.56E-05	1.55E-05	1.91E-03			18
12H-1, 92-94	103.23	8.69E-08	8.69E-05	5.80E-05	1.66E-03			17
12H-2, 95-97	104.76	7.60E-08	7.60E-05	2.32E-05	2.26E-03			19
12H-3, 105-107	106.36	1.43E-07	1.43E-04	4.75E-05	3.03E-03	6.62E-02	5.92E-02	25
12H-4, 98-100	107.79	1.52E-07	1.52E-04	3.73E-05	3.70E-03			22
12H-5, 80-82	109.11	1.18E-07	1.18E-04	2.34E-05	2.49E-03			21
12H-6, 73-75	110.54	1.12E-07	1.12E-04	1.31E-05	2.30E-03			19
12H-7, 50-52	111.81	3.13E-07	3.13E-04	1.67E-05	2.11E-03			18
13H-1, 96-98	112.77	9.63E-08	9.63E-05	8.13E-06	2.41E-03			25
13H-2, 91-93	114.22	5.32E-08	5.32E-05	4.66E-06	1.53E-03			19
13H-3, 86-88	115.67	8.62E-08	8.62E-05	1.97E-05	2.20E-03	3.89E-02	3.59E-02	14
13H-4, 93-95	117.24	7.06E-08	7.06E-05	9.15E-06	2.02E-03			20
13H-5, 93-95	118.74	1.10E-07	1.10E-04	2.24E-05	2.25E-03			35
13H-6, 90-92	120.21	1.08E-07	1.08E-04	1.03E-05	2.33E-03			16
13H-7, 52-54	121.33	2.68E-08	2.68E-05	1.31E-05	2.09E-03			11
14H-1, 94-96	122.25	1.03E-07	1.03E-04	5.35E-05	1.95E-03			16
14H-2, 95-97	123.76	7.18E-08	7.18E-05	1.94E-05	2.16E-03			13
14H-3, 94-96	125.25	1.49E-07	1.49E-04	1.71E-05	2.20E-03	4.09E-02	3.77E-02	19
14H-4, 93-95	126.74	9.99E-08	9.99E-05	2.47E-05	1.78E-03			13
14H-5, 98-100	128.29	6.38E-08	6.38E-05	8.67E-06	1.18E-03			9
14H-6, 97-99	129.78	6.29E-08	6.29E-05	1.56E-05	1.59E-03			6
14H-7, 40-42	130.71	7.96E-08	7.96E-05	1.29E-05	1.64E-03			18
15H-1, 95-97	131.76	7.83E-08	7.83E-05	1.18E-05	1.64E-03			19
15H-2, 93-95	133.24	7.92E-08	7.92E-05	3.00E-05	1.66E-03	2.46E-02	2.26E-02	6
15H-3, 97-99	134.78	1.83E-07	1.83E-04	4.46E-05	1.83E-03			20
15H-4, 95-97	136.26	1.39E-07	1.39E-04	1.91E-05	1.73E-03			19
15H-5, 79-81	137.60	8.72E-08	8.72E-05	1.06E-05	1.74E-03			11
	Mean		1.51E-04	4.13E-05	2.91E-03	4.51E-02	4.10E-02	19
	Minimum		2.68E-05	4.66E-06	1.18E-03	2.46E-02	2.26E-02	1
	Maximum		7.67E-04	1.95E-04	8.45E-03	6.71E-02	6.03E-02	39
	Number		101	101	101	15	15	101

Note: NRM = natural remanent magnetization, RM20 = remanent magnetization after AF demagnetization at 20 mT, ARM = anhysteric remanent magnetization, SIRM = saturation isothermal remanent magnetization, IRM–0.3 = backfield isothermal remanent magnetization induced at -0.3 T, K = magnetic susceptibility.